A New Polycrystalline Co-Ni Superalloy

M. Knop[1], P. Mulvey[1], F. Ismail[1], A. Radecka[1], K.M. Rahman[1], T.C. Lindley[1], B.A. Shollock[1,2], M.C. Hardy[3], M.P. Moody[4], T.L. Martin[4], P.A.J. Bagot[4], D. Dye[1]

[1] *Department of Materials, Royal School of Mines, Imperial College London, Prince Consort Road, London SW7 2BP, UK*

[2] *WMG, University of Warwick, Coventry CV4 7AL, UK*

[3] *Rolls-Royce plc, PO Box 31, Moor Lane, Derby DE24 8BJ, UK*

[4] *Department of Materials, University of Oxford, Parks Road, Oxford OX1 3PH, UK*

Abstract

In 2006, a new ordered $L1_2$ phase, $Co_3(Al,W)$ was discovered that can form coherently in an *fcc* A1 Co matrix. Since then, a community has developed that is attempting to take these alloys forward into practical applications in gas turbines. A new candidate polycrystalline Co-Ni γ/γ' superalloy, V208C, is presented that has the nominal composition 36Co-35Ni-15Cr-10Al-3W-1Ta (at.%). The alloy was produced by conventional powder metallurgy superalloy methods. After forging, a γ' fraction of $\sim 56\%$ and a secondary γ' size of 88 nm were obtained, with a grain size of 2.5 µm. The solvus temperature was 1000°C. The density was found to be $8.52\,\mathrm{g\,cm^{-3}}$, which is similar to existing Ni alloys with this level of γ'. The alloy showed the flow stress anomaly and a yield strength of 920 MPa at room temperature and 820 MPa at 800°C, similar to that of Mar-M247. These values are significantly higher than those found for either conventional solution and carbide strengthened Co alloys or the γ/γ' Co superalloys presented in the literature thus far. The oxidation resistance, with a mass gain of $0.08\,\mathrm{mg\,cm^{-2}}$ in 100 h at 800 °C, is also comparable to that of existing high temperature Ni superalloys. These results suggest that Co-based and Co-Ni superalloys may hold some promise for the future in gas turbine applications.

1. Introduction

Nickel-base superalloys are widely used in the hot section of gas turbines, due to their outstanding balance of high temperature oxidation and corrosion resistance, strength, creep resistance and fatigue performance. Much academic attention is paid to alloys for hollow single crystal blades, which are produced by Bridgman casting, coated with a thermal barrier coating and further protected from the hot gas stream by bleed air film cooling. Potentially of equal engineering importance, however, are polycrystalline static structures and disc rotors. These are typically uncoated and, in addition to creep resistance at the rim, must also have good strength, fatigue resistance and toughness. However, they are only required to sustain rim temperatures of around 700-800 °C, as opposed to blades which operate in a gas stream that is significantly above their melting point. The most modern such disc alloys are fabricated by powder metallurgy from inert gas atomised powders.

In common with blade alloys, there is a concern that the temperature capability of Ni polycrystalline static structure and disc alloys is reaching a plateau. This puts at risk continuing improvements in gas turbine operating efficiency, which from a thermodynamic standpoint is limited by the turbine entry temperature. With global air travel demand exhibiting long term growth rates of around 6% p.a. and concerns over CO_2 emissions and so-called 'peak oil,' there is a strong driver for alloys with enhanced temperature capability which retain a reasonable balance of mechanical properties, oxidation resistance and density. Fuel efficiency is also a key differentiator for gas turbine manufacturers in the market and a strong determinant of airline profitability, to the extent that old aircraft are often retired after only 20 years, long before the end of their service life.

Therefore, it was fortunate that in 2006, Sato *et al.* announced the discovery of a new potential superalloy system [1], in which a ductile intermetallic cubic phase precipitates coherently from its parent cubic matrix, based on the newly-discovered $L1_2$ $Co_3(Al,W)$ precipitate in an A1 *fcc* Co matrix. Since then, several groups worldwide have been developing this alloy system, in most instances for blade alloys. The great advantage of the $Co_3(Al,W)$ system would seem to be the slow diffusion rate and low solubility of W in the matrix, limiting coarsening, which might enable greater endurance at higher temperatures. From a casting perspective the freezing range is reduced, as pointed out by Tsunekane *et al.* [2], which may be of interest for very large cast industrial gas turbine blades and guide vanes. To date, oxidation resistance has proved to be a challenge, although B appears to have a substantial beneficial effect, as does Cr [3].

The flow stress anomaly (increasing yield strength with

temperature) has been observed [4], however, most of the Co superalloys presented to date have relatively low solvus temperatures compared to Ni superalloys with the same volume fraction of γ'. In addition, the Co superalloys show a positive misfit, δ, in excess of 0.5%, where $\delta = 2(a_{\gamma'} - a_\gamma)/(a_\gamma + a_{\gamma'})$. In Ni superalloys, creep performance generally improves as the misfit decreases, because the concomitant reduction in surface energy reduces the driving force for coarsening. Retaining a fine γ' distribution is important in creep because restricting the γ channel width acts to increase the bowing stress of the mobile dislocations and thereby strengthen the alloy [5]. In the high stress case of particle shearing below 750°C, the high misfits will also give rise to misfit strengthening, but in Ni superalloys, the main strengthening effect in the case of cutting is from the antiphase boundary energy associated with the requirement to pass the *fcc* dislocations through the precipitate in pairs or even dislocation ribbons [6–8].

As previously mentioned, the deleterious effects of high misfit will be mitigated by the low diffusivity of W in the γ. This also has the side effect of requiring long ageing times in many academic studies in order to produce γ' precipitates that are large enough to image satisfactorily. In industrial practice it would be desirable to avoid such expensive heat treatments, and to retain a fine γ' distribution.

Over the last several years, we have been exploring whether viable polycrystalline Co-base superalloys can be produced, with improved oxidation resistance and mechanical performance compared to conventional Ni superalloys. The present contribution provides a snapshot of the current status of this work, using the example of a single alloy, V208C, that was subject to patent protection in 2013.

2. Results

2.1. Alloy V208C

V208C's composition is provided in Table 1 [9]. The alloy is designed to have a Co:Ni ratio of just greater than 1.0. Shinagawa *et al.* [10] showed that a continuous phase field exists between each of the γ' $L1_2$ Ni_3Al and $Co_3(Al,W)$ phases, such that a $(Co,Ni)_3(Al,W)$ γ' phase can be precipitated from a γ A1 (*fcc*) matrix. In the Ni-free case, Yan *et al.* [11] and Bauer *et al.* [12] showed that additions of significant amounts of Cr destabilise the γ' phase, and there is increasing evidence that Co – $Co_3(Al,W)$ microstructures can be metastable, decomposing to Co – CoAl – Co_3W at long ageing times. Therefore Ni additions act to widen the γ' phase field, increase the stability of the γ', and simultaneously allow for the addition of Cr to provide oxidation resistance.

Most of the Co superalloys presented to date [2, 4, 12] have been targeted at single crystal turbine blade applications, and have compositions in the region of Co-10Al-9(W+Ta) (at.%). Such high refractory metal contents result in an alloy density of over $9\,\mathrm{g\,cm^{-3}}$, whereas alloys for disks in particular usually have densities of $< 8.5\,\mathrm{g\,cm^{-3}}$. Therefore in the present case an additional benefit of the introduction of Ni is that it shifts the γ' stoichiometry to higher Al contents, allowing a reduction in the overall alloy density, to $8.52\,\mathrm{g\,cm^{-3}}$ for the present alloy. For comparison, LSHR [13] has a density that is 2% lower, of $8.35\,\mathrm{g\,cm^{-3}}$.

	Co	Ni	Cr	Al	W	Ta	C	B	Zr
wt.%	35.9	33.9	13.0	4.78	9.3	3.0	0.03	0.04	0.07
at.%	36.1	34.2	14.8	10.5	3.0	1.0	0.15	0.20	0.04

Table 1: Measured composition (ICP-OES, Incotest, Hereford, UK) of the alloy V208C.

Meher *et al.* also found [14] that in the Co – $Co_3(Al,W)$ case, significant solubility of W in the matrix remained, which has the benefit of allowing for some solid solution strengthening of the matrix. In a similar way, the solubility for Al in Co is significantly higher than in Ni, and so Co matrices allow for density reduction by permitting a greater Al content than would otherwise be the case.

Therefore, the use of a 1:1 Co/Ni ratio in the present alloy represents a balance that aims to simultaneously fulfil the demand for corrosion resistance, density and matrix strength, whilst retaining the benefit of having a high refractory metal content in the γ' phase which is the fundamental attraction of Co-base γ/γ' superalloys over Ni-base superalloys.

The alloy powder was manufactured by vacuum induction melting and inert gas atomisation, and then consolidated by hot isostatic pressing (HIP) by ATI Powder Metals, Pittsburgh, PA, USA. It was then isothermally forged by ATI Ladish Forging, Cudahy, WI, USA. After forging, the material was subjected to a heat treatment of 1050°C

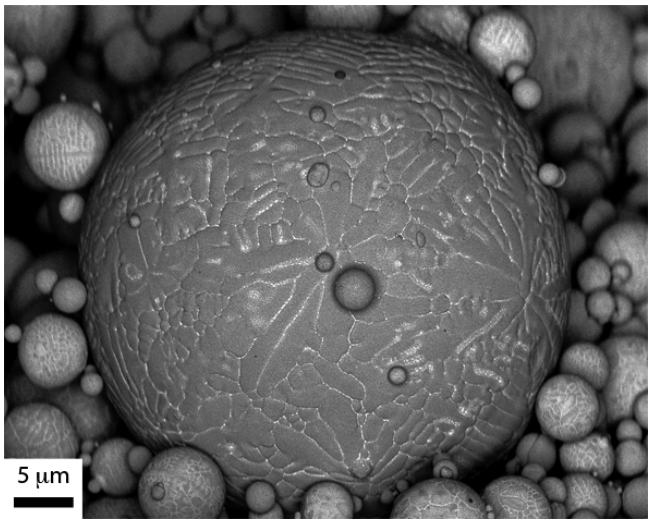

Figure 1: The as-sprayed over- and under-sized gas atomised powder, observed using backscatter electron imaging.

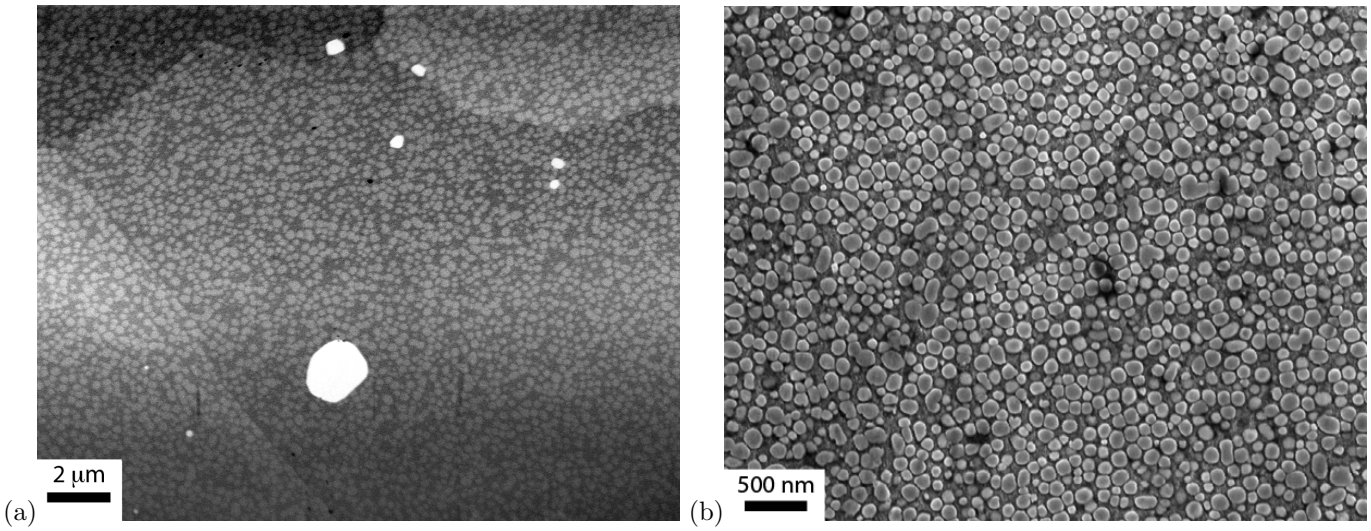

Figure 2: As-HIP, forged and heat treated microstructure of the alloy produced, (a) observed in backscatter electron imaging to highlight secondary phases such as carbides and (b) etched secondary electron image to highlight the γ' distribution.

for 30 min, above the solvus temperature of 1000°C.

2.2. Alloy microstructure

The gas atomised powder is shown in Figure 1; the sample examined is from the over-and under-sized powder that was retained for examination. Small satellite powder particles can be observed on the larger particles, and solidification segregation can be observed in backscatter electron imaging (Z-contrast). The very fine dendrite arm spacing provides an indication of the high solidification rates that occur during powder processing, which act to minimise, but not completely eliminate, such microsegregation. During properly designed HIP cycles, homogenisation of this microsegregation occurs such that a homogenous, low grain size alloy product is obtained.

The option of forging from the as-HIP condition breaks up networks of high oxygen, oxy-carbide prior particle boundaries (PPBs) by introducing high levels of deformation to cause recrystallisation. Otherwise, these can give rise to poor tensile, creep and fatigue performance. The microstructure produced is provided in Figure 2. The small submicron precipitates observed in backscatter images are expected to be carbides. The etched secondary electron image provides an improved view of the γ' structure. The secondary γ' observed have a volume fraction of $\sim 56\%$ and an average diameter of 88 nm.

The grain structure has also been observed by EBSD, Figure 3, showing an average grain size of 2.5 µm and a mild forging texture; as the sample has recrystallised the texture is still quite mild ($< 2.5\times$ random). The grain size distribution was obtained by fitting a Weibull distribution to the cumulative distribution function, giving a (number) average grain size of 2.5 µm, which is comparable to that typically obtained for extruded powder metallurgy (P/M) Ni superalloys.

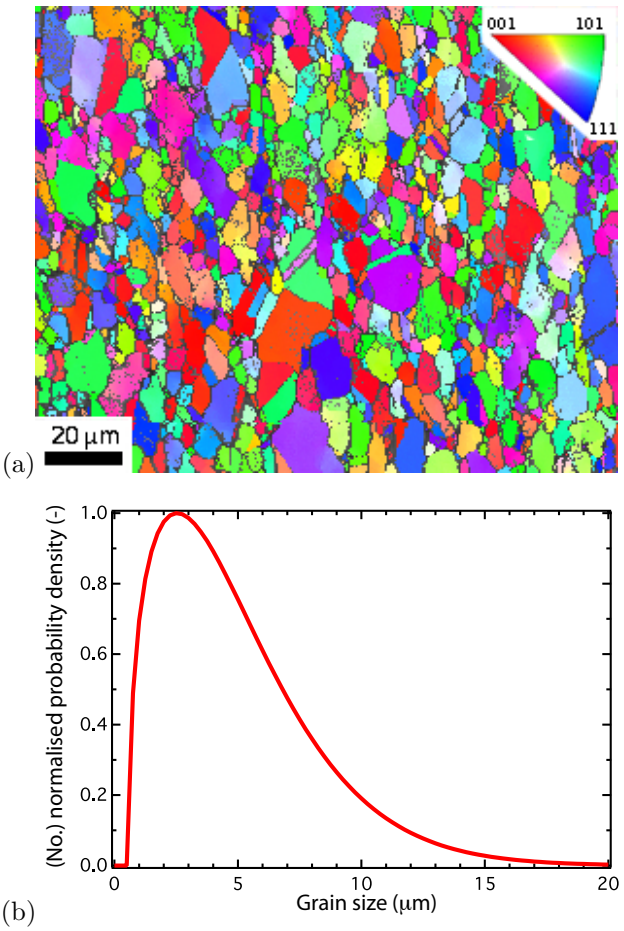

Figure 3: Inverse Pole Figure (IPF) coloured, overlaid with band contrast, electron backscatter diffraction (EBSD) image of the microstructure, together with the grain size distribution obtained (0.5 µm step size, 3.6×10^5 points, 785 grains).

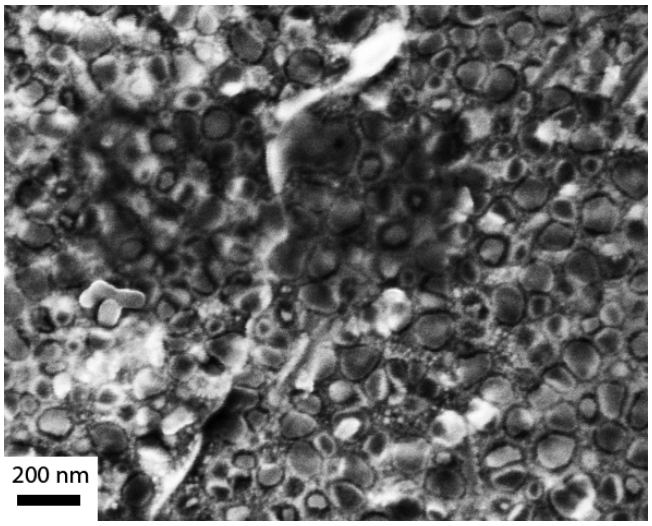

Figure 4: Example of a serrated grain boundary producing by slow cooling from super-solvus heat treatment (etched secondary electron imaging, running top-to-bottom).

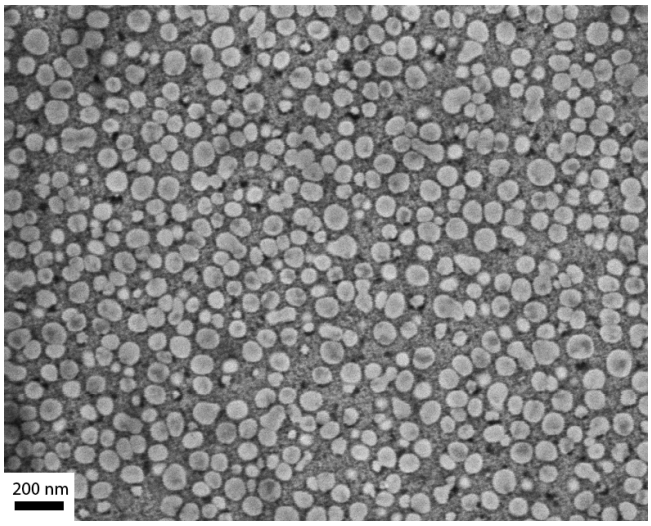

Figure 5: Effect of 850°C heat treatment on the as-forged γ' microstructure; a reduction in the secondary γ' fraction is observed, against a background of ~ 10 nm tertiary γ' that formed on low temperature ageing heat treatment (etched secondary electron imaging).

Slow cooling from heat treatment temperatures just above or below the solvus is often applied to produce serrated grain boundaries in high temperature Ni superalloys [15]. The concept is that grain boundary serrations are supposed to inhibit grain boundary sliding in high temperature creep conditions, in a similar way to $M_{23}C_6$ carbides. In the present case of V208C, serrated grain boundary microstructures can also be achieved, Figure 4.

Very frequently, prior to service a lower temperature heat treatment will be applied, in part to relax away residual stresses and also to stabilise the initial γ' distribution. The effect of such a heat treatment is shown in Figure 5. It can be observed that the secondary γ' fraction is reduced, replaced with fine scale tertiary γ'.

2.3. Phase metallurgy

Atom probe tomography experiments were performed on samples in the forged condition, Figure 6. Specimens were prepared using an FEI Helios NanoLab 600 DualBeam system equipped with an Omniprobe^{TM}. A detailed description of the liftout and tip sharpening procedure can be found elsewhere [16–18]. All atom probe experiments were performed in the laser mode using a LEAP 3000X HR at the Department of Materials, University of Oxford at a temperature of 50 K and pulse energy of 0.3 nJ. A total of 34×10^6 ions were detected and reconstructed using the IVAS^{TM}software with a 13 at.% Cr isosurface to define the precipitates observed. These allowed the average composition of the secondary γ' precipitates to be determined. For the matrix, a manually selected subset of 12×10^6 ions was used, and the composition of both secondary γ' and the matrix are shown in Table 2. Composition profiles were generated using the proxigram approach [19], Figure 7. Comparing these measured compositions to the alloy, they

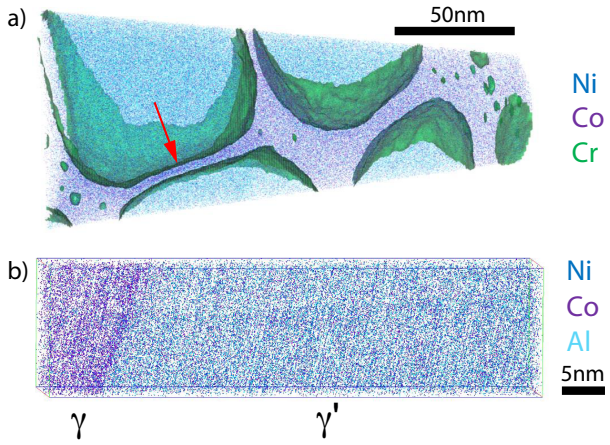

Figure 6: (a) Atom probe tomogram of the V208C needle, with the 13 at.% Cr isosurface highlighted to illustrate the γ' precipitates. The arrow shows the interface examined in (b), illustrating the {100} atomic planes.

	Co	Ni	Cr	Al	W	Ta
secondary γ'	25.2	48.5	4.7	16.6	3.3	1.7
matrix γ	44.8	23.8	24.6	4.7	2.0	0.1
$k = C_{\gamma'}/C_{\gamma}$	0.56	2.0	0.19	3.5	1.7	∼17

Table 2: Atom probe tomography measurements of the compositions of the secondary γ' (identified using a 13.5 at.% Cr isosurface) and of the matrix excluding the tertiary γ', in at.%, together with the inferred partition coefficients k (2 s.f.).

are generally consistent with a γ' volume fraction of 45–55%, which is similar to that measured by microscopy.

Previously, Meher *et al.* have performed measurements

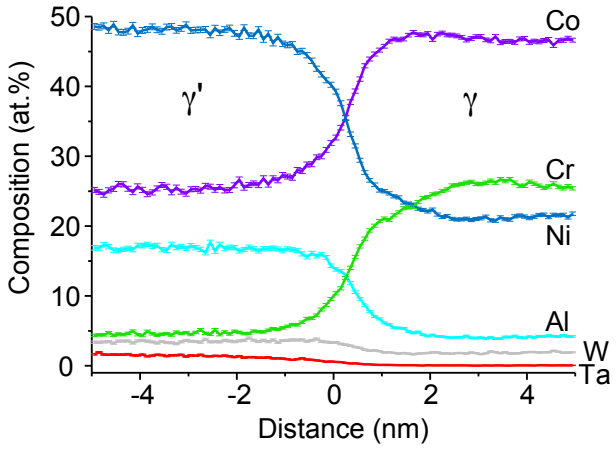

Figure 7: Composition profile across the γ/γ' interface derived using the proxigram approach, for the secondary γ'. An interface width in excess of 1 nm can be observed.

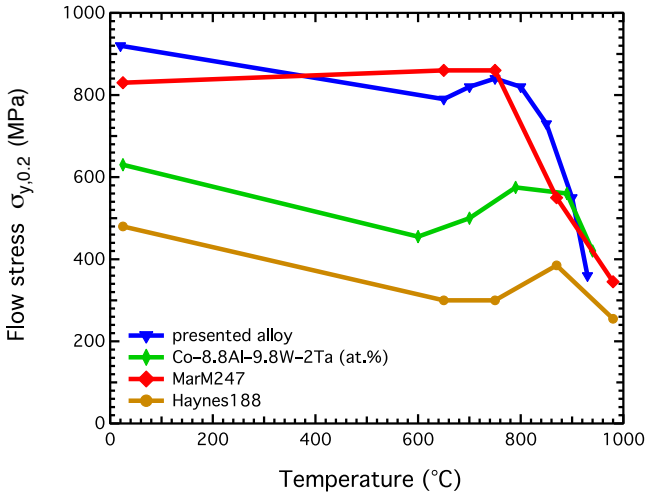

Figure 8: Flow stress behaviour with temperature, measured using isothermal compression testing at a strain rate of $1 \times 10^{-3}\,\mathrm{s}^{-3}$, compared to data from Suzuki *et al.* [23].

for Co-9Al-10W-2Ta (at.%) [14, 20], and Hwang *et al.* have performed measurements in the conventional Ni-base P/M polycrystalline alloy René 88DT (56Ni-13Co-18Cr-4.5Al-4.5Ti-1.2W-0.5Nb-2.4Mo-0.15C-0.08B-0.02Zr, at.%) [21, 22]. These provide a comparison for cases closer to end-member Co- and Ni-base superalloys to compare to the 1:1 Co:Ni ratio employed here.

Partitioning of Co to the γ phase is observed, an approximate 2:1 ratio between Co and Ni in both the γ and γ' phases. This means that the Co/Ni site in the γ' is approximately two-thirds Ni. Correspondingly, the W content in the γ' is reduced from $\sim 12\%$ found in Co-Al-W, as is the matrix solubility for W ($\sim 5\%$ in Co-Al-W), due to the lower W contents used in the alloy overall.

In Co-Al-W alloys, the Al content in the matrix and precipitate are found to be very similar, at around 10-12% ($k = 1.1$), whereas Al partitions to the γ' much more strongly in Ni superalloys, $k \sim 8$. In the present case intermediate behaviour is observed, $k = 3.5$, which is consistent with the observations of Shinagawa [10], as are the results for the dependence of Co partitioning on Ni content. Ta strongly partitions to the γ' and is a very strong γ' former, as in the Co-Al-W situation.

It is striking that Cr is a very strong γ former, $k = 0.2$, although the effect is less pronounced than in Ni superalloys, where $k < 0.1$. Here it should be recalled that in both conventional solid solution, carbide strengthened Co superalloys, such as Haynes 188, and Ni disc alloys, the γ matrix will often contain > 25 at.% Cr. What is different in the present case is that around 5% Cr exists in the γ', compared to only 2 at.% in René 88DT, which implies that Co-Ni superalloys should be able to tolerate higher levels of Cr at a given γ' content than conventional high temperature Ni alloys, and hence possess better oxidation resistance (below the point at which chromia volatilises, $> 1000\,^{\circ}\mathrm{C}$).

2.4. Mechanical behaviour

The flow stress ($\sigma_{y,0.2}$) dependence with temperature of V208C was measured in isothermal compression, in the forged and heat treated (1050°C for 30 min), serrated grain boundary condition, Figure 8. A room temperature (RT) flow stress of 920 MPa was obtained with 820 MPa at 800°C. The flow stress anomaly was also observed. It should be recalled that the flow stress anomaly is attributed to the cross-slip of dislocations from the octahedral to the cube plane, causing the formation of Kear-Wilsdorf locks, and that this phenomenon breaks down when thermally activated slip on the cube place becomes preferred (for a fuller discussion, see, *e.g.* [22]). Compared to the alloys reported by Suzuki *et al.* [23], the strengths obtained here are significantly greater, and similar to those found for a high γ' directionally solidified Ni blade alloy such as Mar M247 (although in both those cases the alloys concerned lack grain size strengthening).

Significantly, the temperature at which the flow stress anomaly breaks down is even higher than for Mar M247, despite that alloy's very high solvus temperature ($\sim 1200\,^{\circ}\mathrm{C}$) [24] compared to that of the present alloy (1000°C). Therefore, it appears that high-Co, high-W γ' only begins to suffer from the breakdown of Kear-Wilsdorf locks at a higher temperature than in case of Ni-Al γ'. This might be explained by the fact that W will tend to restrict diffusion and hence thermally activated slip.

2.5. Oxidation behaviour

$10 \times 10 \times 2$ mm samples of V208C were subjected to isothermal oxidation in laboratory air for 100 h at 800°C; an areal mass gain of $0.08\,\mathrm{mg\,cm^{-2}}$ was obtained, at the limit of measurement accuracy for intermittent weighing. A previous alloy of ours [25] containing 12 at.% Cr showed a mass gain of $0.29\,\mathrm{mg\,cm^{-2}}$ in the same conditions. These

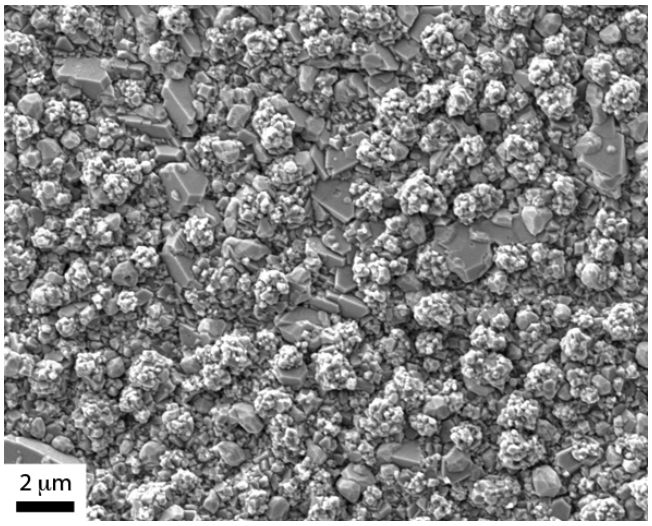

Figure 9: Oxide scale formed on the surface of V208C after 400 h oxidation in laboratory air at 800°C (secondary electron imaging).

results are encouraging relative to the value of $3\,\mathrm{mg\,cm^{-2}}$ obtained for Co-9Al-9W-0.12B (at.%) by Klein *et al.* [3].

The oxide scale obtained from the polycrystalline alloy after 400 h is shown in Figure 9. Two distinct crystalline oxide forms can be observed on the surface, supported by SEM-EDX analysis; a facetted oxide the with approximate composition 22Al-10(Co+Ni)-68O (at.%), and a nodular oxide with the approximate composition 12Al-12Cr-12(Co+Ni)-64O, which are both suspected to be spinels. Cross-sectional analysis in the TEM is ongoing, but it appears that the oxide scale formed at 200 h had not yet reached a stage of equilibrium oxide growth, with the appearance of continuous Al_2O_3 and Cr_2O_3 layers. The appearance of such layers underlying a surface spinel was observed by Yan *et al.* in our previous, less oxidation-resistant, alloy Co-7Al-7W-10Cr (at.%) [26], which showed an areal mass gain of $2.0\,\mathrm{mg\,cm^{-2}}$ in 100 h at 800°C.

3. Discussion and Outlook

At this stage, together with the work published by Titus *et al.* [27–29], Suzuki *et al.* [4, 23, 30], Shinagawa *et al.* [10, 31] and Klein *et al.* [3, 32], the following observations about the prospects for the development of Co-Al-W and Co-Ni-Cr-Al-W alloys can be made. The flow stress anomaly has been observed by several groups, but at similar temperature to those found for Ni-base superalloys. Minimum creep rates as low as $10^{-8}\,\mathrm{s^{-1}}$ at 900°C and 310 MPa have been reported [27, 29] for the single crystal alloy Co-29Ni-9.8Al-6.3W-2.4Ta-6.4Cr (at.%), which is similar to the performance of René N4, a modern Ni turbine blade alloy.

Oxidation performance similar to that of modern Ni disc alloys also appears to be attainable; given that oxidation damage is heavily implicated in low cycle fatigue degradation [33, 34] then this must be an essential precondition for the production of fatigue-resistant alloys. Since density directly impacts upon weight and upon the centrifugal loads that have to be sustained in service, the high density associated with high W contents is detrimental, but it appears that alloys can be produced with similar densities to current high temperature alloys for blades, static parts and discs.

The solvus temperatures attained remain similar, or even slightly lower, than those for competitor Ni superalloys, and the freezing ranges are substantially reduced. Whilst both these factors have benefits for processability, a concern would be that the amount of γ' present at service temperatures may be limited compared to that observed at room temperature; therefore higher solvus temperatures are desired. This will entail adding γ' formers such as Al, W, Ta, Ti and Nb [10, 11, 35, 36]. Nevertheless, in the case of Ni superalloys, matrix strength is also a key requirement and this is the reason for the addition of 2.7 and 3.8 wt.% Mo in LSHR and ME3, respectively [22]. In addition, probably slightly greater room temperature strength is required, at least in the case of disc alloys.

In summary, while the results that we and others have obtained to date are promising in that similar properties to Ni superalloys appear to be attainable, whether superior Co- or Co-Ni superalloys will eventually turn out to be attainable is unknown at this time. Nevertheless, 9 years on from the first report of the $Co_3(Al,W)$ phase, substantial progress has been made. It should be recalled that even if only similar properties can be obtained, the additional flexibility provided to the alloy designer should enable different balances of properties to be obtained. Across the engine, this might allow different alloys to be better tailored for different applications requiring strong and ductile, creep and fatigue resistant materials that can endure harsh oxidising and sulphidising conditions. Therefore at this stage it seems likely, as has been reported by Ishida [37], that Co-base superalloys will eventually be employed in at least some applications in gas turbines.

4. Conclusions

Results for a polycrystalline Co-Ni superalloy, V208C, have been presented. The alloy shows good oxidation resistance, $0.08\,\mathrm{mg\,cm^{-2}}$ mass gain after 100 h at 800°C, a density of $8.52\,\mathrm{g\,cm^{-3}}$, a γ' solvus of 1000°C and a room temperature flow stress of 920 MPa. The flow stress anomaly was observed, with a secondary γ' fraction of $\sim 56\%$ and average size of 88 nm. Substantial partitioning of Co to the γ and Ni to the γ' was observed (around 2:1 in each case). The solubility of Cr in the γ', 4.7 at.%, was greater than in the case of Ni superalloys. Al showed similar partitioning to that observed in Ni superalloys, and substantial solubility for W in the γ (2 at%) was observed. As in Ni superalloys, serrated grain boundaries and bimodal γ/γ' distributions could be produced if desired.

While the present alloy is only an early attempt, it appears that it may be possible to develop Co-Ni superalloys that are attractive for gas turbine applications.

Acknowledgements

The authors would like to acknowledge the financial support provided by Rolls-Royce plc, Imperial College London and EPSRC (UK) grant EP/H022309/1. Useful conversations with Drs Vassili Vorontsov, Hui-Yu Yan (Imperial) and Howard Stone (Cambridge) are also acknowledged.

References

[1] J. Sato, T. Omori, K. Oikawa, I. Ohnuma, R. Kainuma, and K. Ishida. *Science*, 312:90–91, 2006.
[2] M. Tsunekane, A. Suzuki, and T.M. Pollock. *Intermetallics*, 19:636–643, 2011.
[3] L. Klein, Y. Shen, M.S. Killian, and S. Virtanen. *Corros Sci*, 53:2713–2720, 2011.
[4] A. Suzuki, G. C. DeWolf, and T. M. Pollock. *Scripta Mater*, 56:385–388, 2007.
[5] T.M. Pollock and A.S. Argon. *Acta Metall Mater*, 40:1–30, 1992.
[6] L. Kovarik, R.R. Unocic, Ju Li, C. Shen, Y. Wang, and M.J. Mills. *Prog Mater Sci*, 54:839–873, 2009.
[7] V.A. Vorontsov, L. Kovarik, M.J. Mills, and C.M.F. Rae. *Acta Mater*, 60:4866–4878, 2012.
[8] C.M.F. Rae and R.C. Reed. *Acta Mater*, 55:1067–1081, 2007.
[9] D. Dye, M. Knop, H.-Y. Yan, M.C. Hardy, and H.J. Stone, Gamma prime strengthened cobalt & nickel based superalloy. GB Patent application 1312000.1, 2013.
[10] K. Shinagawa, T. Omori, J. Sato, K. Oikawa, I. Ohnuma, R. Kainuma, and K. Ishida. *Mater Trans*, 49(6):1474–1479, 2008.
[11] H.-Y. Yan, V.A. Vorontsov, and D. Dye. *Intermetallics*, 48:44–53, 2014.
[12] A. Bauer, S. Neumeier, F. Pyczak, and M. Göken. In E.S. Huron, R.C. Reed, M.C. Hardy, M.J. Mills, R.E. Montero, P.D. Portella and J. Telesman (eds.), *Superalloys 2012*, pp 695–703, Seven Springs, PA, USA, 2012. TMS, Wiley.
[13] T.P. Gabb, J. Gayda, J. Telesman, and P. Kantzos. Thermal and mechanical property characterization of the advanced disk alloy LSHR (No. NASA/TM2005-213645). Technical report, NASA, 2005.
[14] S. Meher, H.Y. Yan, S. Nag, D. Dye, and R. Banerjee. *Scripta Mater*, 67:850–853, 2012.
[15] R.J. Mitchell, H.Y. Li, and Z.W. Huang. *J Mater Process Tech*, 209:1011–1017, 2009.
[16] A. Cerezo, P.H. Clifton, M.J. Galtrey, C.J. Humphreys, T.F. Kelly, D.J. Larson, S. Lozano-Perez, E.A. Marquis, R.A. Oliver, G. Sha, K. Thompson, M. Zandbergen, and R.L. Alvis. *Mater Today*, 10(12):36, 2007.
[17] T.F. Kelly and D.J. Larson. *Materials Charact*, 44(1-2):59–85, 2000.
[18] K. Thompson, D. Lawrence, D.J. Larson, J.D. Olson, T.F. Kelly, and B. Gorman. *Ultramicroscopy*, 107(2-3):131–139, 2007.
[19] O.C. Hellman, J.A. Vandenbroucke, J. Rüsing, D. Isheim, and D.N. Seidman. *Microsc Microanal*, 6(5):437–444, 2000.
[20] S. Meher and R. Banerjee. *Intermetallics*, 49:138–142, 2014.
[21] J.Y. Hwang, R. Banerjee, J. Tiley, R. Srinivasan, G.B. Viswanathan, and H.L. Fraser. *Metall Mater Trans A*, 40(1):24–35, 2009.
[22] R.C. Reed. *The Superalloys - Fundamentals and Applications*. Cambridge University Press, 1st edition, 2006.
[23] A. Suzuki and T. M. Pollock. *Acta Mater*, 56:1288–1297, 2008.
[24] M.J. Donachie. *Superalloys: A Technical Guide*. ASM International, 2002.
[25] M. Knop, V.A. Vorontsov, M.C. Hardy, and D. Dye. In *Proceedings of Eurosuperalloys 2014*, Hyeres, France, 12-16 May 2014.
[26] H.-Y. Yan, V.A. Vorontsov, and D. Dye. *Corros Sci*, 83:382–395, 2014.
[27] M.S. Titus, A. Suzuki, and T.M. Pollock. *Scripta Mater*, 66:574–577, 2012.
[28] M.S. Titus, A. Suzuki, and T.M. Pollock. High temperature creep of new $L1_2$ containing cobalt-base superalloys. In E.S. Huron, R.C. Reed, M.C. Hardy, M.J. Mills, R.E. Montero, P.D. Portella and J. Telesman (eds.), *Superalloys 2012*, pp. 823–832, Seven Springs, PA, USA, 2012. TMS, Wiley.
[29] Y.M. Eggeler, M.S. Titus, A. Suzuki, and T.M. Pollock. *Acta Mater*, 77:352–359, 2014.
[30] T. M. Pollock, J. Dibbern, M. Tsunekane, and A. Suzuki. *JOM*, 62(1):58–63, 2010.
[31] K. Shinagawa, T. Omori, K. Oikawa, R. Kainuma, and K. Ishida. *Scripta Mater*, 61:612–615, 2009.
[32] L. Klein, A. Bauer, S. Neumeier, M. Göken, and S. Virtanen. *Corros Sci*, 53:2027–2034, 2011.
[33] H.S. Kitaguchi, H.Y. Li, H.E. Evans, R.G. Ding, I.P. Jones, and P. Baxter, G. Bowen. *Acta Mater*, 61:1968–1981, 2013.
[34] R. Jiang, S. Everitt, M. Lewandowski, N. Gao, and P.A.S. Reed. *Int J Fatigue*, 62:217–227, 2014.
[35] M. Ooshima, K. Tanaka, N.L. Okamoto, K. Kishida, and H. Inui. *J Alloy Compd*, 508(1):71–78, 2010.
[36] A. Bauer, S. Neumeier, F. Pyczak, and M. Göken. *Scripta Mater*, 63:1197–1200, 2010.
[37] K. Ishida. Recent Progress in Co-base Superalloys - Phase Equilibria and Applications. In *Proceedings of Eurosuperalloys 2014*, Hyeres, France, 12-16 May 2014.